Modeling of Rayleigh Scattering Imaging of Detonation Waves

Guillaume Bechon[1,2], **Rémy Mével**[2], **Dmitry Davidenko**[3], **Joseph Shepherd**[2]

[1]École Polytechnique, Palaiseau, France
[2]California Institute of Technology, Pasadena, USA
[3]ICARE-CNRS, Orléans, France

1 Introduction

Austin et al. [1] and Pintgen et al. [2] performed simultaneous visualization of the shock front and the reaction zone using Schlieren and planar laser-induced fluorescence (PLIF) techniques. Later, Mével et al. [3] continued this work in comparing post-processed numerical simulation results on detonation waves with these previous experimental visualizations of detonations in hydrogen-oxygen-diluent mixtures. These visualization methods permitted to image the reaction zone structure of the detonation front, but the strong attenuation of the incident laser light, due to the absorption at the detonation front, prevents from imaging regions of high OH concentration away from the front. Rayleigh scattering imaging, however, is based on a different phenomenon and could be used to investigate the dynamics of the flow at and behind the detonation front.
In the present study, a wavelength and temperature-dependent Rayleigh scattering cross-section database has been created. After its validation against the data from the literature, this database was used to post-process one-dimensional and two-dimensional detonation simulations in order to compute the Rayleigh scattering intensity in a detonation wave. These simulations were compared to experimental Rayleigh images obtained by Anderson and Dabora [4].

2 The Rayleigh cross-section database development

2 Fundamentals of Rayleigh scattering

The Rayleigh scattering intensity I_{Ray} can be defined as the number of photons per second diffused by a volume V of gas, and collected within the solid angle Ω (along an axis perpendicular to the direction of propagation of the incident light and the direction of its polarization) [5] [6]:

$$\mathbf{I_{Ray}} = \mathbf{k\,\Omega\,V\,I_{0,S}\,N}\,\frac{\partial\sigma}{\partial\mathbf{\Omega}} \tag{1}$$

where $I_{0,S}$ is the intensity of the incident light in $photons^{-1}m^{-2}$, N the density number and k is a system calibration constant which accounts for the optical collection and transmission efficiencies. Thus, in order to compute the Rayleigh intensity, the density and the Rayleigh differential cross-section are needed.

Correspondence to: mevel@caltech.edu

The differential cross-section depends on the position of the detector, the wavelength λ, of the laser light, and the optical properties of the gas [7]. It can be calculated using

$$\frac{\partial\sigma}{\partial\Omega} \approx \frac{4\pi^2(n-1)^2}{\lambda^4 N^2}\sin^2\phi\frac{3}{3-4\rho} \tag{2}$$

where N is the density number, ϕ is the angle of refraction defined as the angle between the polarization direction and the observation direction, ρ is the depolarization factor

$$\rho = \frac{6\gamma^2}{45a^2+7\gamma^2}, \tag{3}$$

with the linear polarizability

$$a^2 = \frac{1}{9}(\alpha_{11}+\alpha_{22}+\alpha_{33})^2, \tag{4}$$

and the anisotropy

$$\gamma^2 = \frac{1}{2}\{(\alpha_{11}-\alpha_{22})^2+(\alpha_{22}-\alpha_{33})^2+(\alpha_{33}-\alpha_{11})^2+6(\alpha_{12}^2+\alpha_{23}^2+\alpha_{31}^2\}. \tag{5}$$

α_{ij} are the polarizability tensor elements.
To simplify this equation, the case $\phi = \frac{\pi}{2}$, where the differential cross-section is maximum, is usually considered. Using the Lorenz-Lorentz equation to replace the index of refraction by the linear polarizability we finally found:

$$\frac{\partial\sigma}{\partial\mathbf{\Omega}} \approx \frac{\mathbf{16\pi^4}}{\lambda^4}\mathbf{a^2F} \tag{6}$$

with $F = \frac{3}{3-4\rho} \approx 1+\frac{7\gamma^2}{45a^2}$ the King factor and a the linear polarizability (in m^3).
Considering a mixture of gaseous species, Equation 7 has to be taken into account [7]:

$$\frac{\partial\sigma}{\partial\mathbf{\Omega}} = \sum_{\mathbf{i=1}}^{\mathbf{n}}\mathbf{X_i}\frac{\partial\sigma_\mathbf{i}}{\partial\mathbf{\Omega}} \tag{7}$$

where X_i is the molar fraction of the species i.

2 Creation of the database

The database was created using the quantum chemistry software *Gaussian03*, which can compute wavelength dependent polarizability tensor. The method used was **B3LYP** and the basis set chosen was **aug-cc-pVTZ**. This database contains the complete polarizability tensor at 12 different wavelengths for 30 species. It was validated against the experimental refractivity data collected by Gardiner et al. [9], the depolarization ratio data of Fielding et al. [10] and the cross-section data of Sutton et al. [11]. A comparison with Gardiner et al. data was done for 26 species and for six different wavelengths. With these method and basis set, the mean relative error is 10% and the average relative error for the species of the H_2-O_2 chemical system is 13%. The comparison with Fielding et al. and Sutton et al. work gave comparable relative errors. An illustration of these comparisons is displayed in Figure 1 a) to c).

As *Gaussian* does not permit to compute temperature-dependent polarizability tensor, we analysed the results of Sutton and Driscoll [11], Zhao and Hiroyasu [5], Graham et al. [12] and Holm and Kerl [13], to establish a wavelength-dependent law for the variation of the cross-section with temperature, $\Delta\sigma_T$, as shown in Figure 1 d).

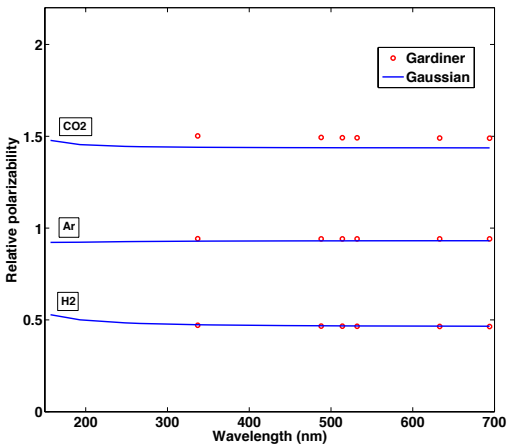

a) Polarizabity for Ar, H_2O and H_2

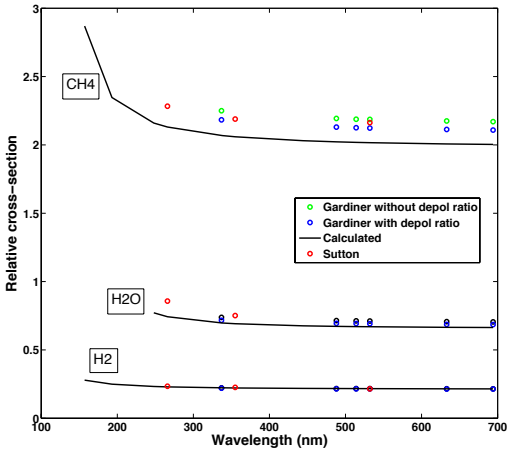

b) Relative cross-section for H_2, H_2O and CH_4

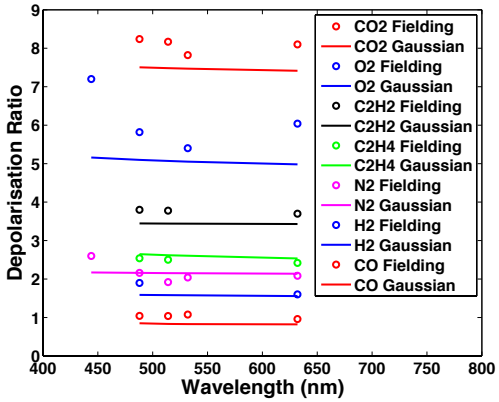

c) Depolarization ratio

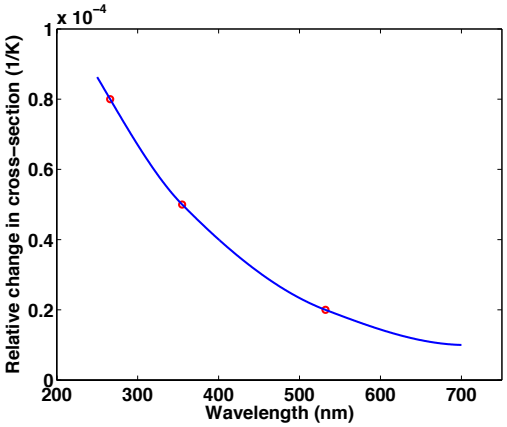

d) wavelength dependent law for $\Delta\sigma_T$

Figure 1: Validation of the database against data from a) Gardiner et al. [9], b) Sutton and Driscoll [11], and c) Fielding et al. [10], and Wavelength-dependent law for $\Delta\sigma_T$ d).

3 Application to detonation simulations

In a first time, we performed a direct qualitative comparison between the experimental and calculated Rayleigh images as shown in Figure 2. The most relevant real imaging diagnostic parameters, such as the real resolution of the camera, the spatial distribution of the laser sheet, the dynamical range of the camera, and the attenuation of the laser intensity, have been taken into account to obtain the most realistic image of the detonation front. The experimental image of Anderson et al. has a resolution of 600 μm (each pixel images an area of approximately 60 μm x 60 μm and an average in a 10 pixel range is done to reduce the noise in the image), 256 levels of color and the laser sheet is 30 mm wide. The calculated Rayleigh intensity map compares well with the experimental image. A number of features observed in the experiment are well captured such as the localized very high intensity at the triple points and the high intensity regions located behind the front, between two diverging transverse waves. The length of the region of high intensity behind the incident shock is over-estimated in the simulation.

The present approach could be used for designing a more precise imaging system and access a large range of length scales at and behind the detonation front. This is illustrated in Figure 2 d) for which the characteristics of a PCO2000 CDD camera, available at in our laboratory, were considered to obtain the Rayleigh intensity map from the 2-D simulation results. The resolution taken into account was 7 μm x

7 μm (with averaging, the resolution is 35-70 μm x 35-70 μm), and dynamic range of 14 bits (16384 level of color). The image is much better resolved than in Anderson and Dabora's prioneering study and could enable quantitative validation of detonation simulations performed with detailed chemistry.

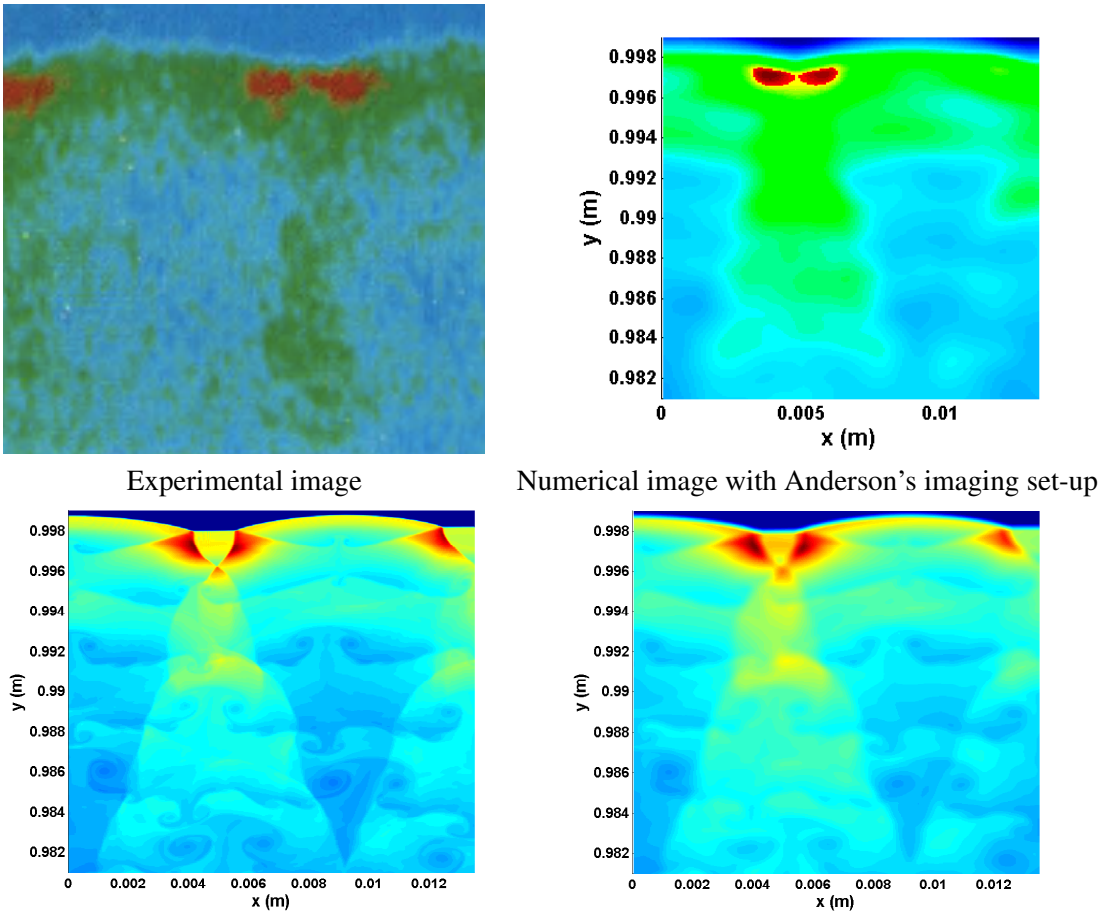

Experimental image | Numerical image with Anderson's imaging set-up

Base numerical image | Image expected with a PCO2000 CDD

Figure 2: Comparison between Anderson et al. experimental image [4] and the post-processed simulation of Davidenko et al. [8].

In a second time, a quantitative comparison between the experimental Rayleigh intensity profiles from Anderson and Dabora [4] and calculated ones has been performed. Both 1-D steady detonation (ZND model), with velocities in the range D/D_{CJ}=0.85-1.2, and 2-D simulations have been considered for this comparison. It is seen in Figure 3 b) that the maximum Rayleigh intensity predicted by the ZND model at D_{CJ} lies in between the experimental values obtained at different locations of the detonation front. The intensity far from the detonation front is well reproduced. The width of the Rayleigh peak appears much thinner in the ZND simulation than in the experiments. These discrepancies between the experimental and calculated Rayleigh profiles are essentially due to the simplified description of the detonation wave structure considered in the ZND model. The experimental profiles have been obtained at different instants of the cellular cycle and thus for different shock velocities and shapes (curvatures). In order to account for the effect of the detonation front velocity, the Rayleigh intensity has been calculated for several velocities around the Chapman-Jouguet velocity as shown in Figure 3 a) for D/D_{CJ}=0.85 and c) for D/D_{CJ}=1.2. Concerning the peak intensity, the ZND model is closer to the highest experimental value for the over-driven case whereas for the under-driven case, it is closer to the lowest

experimental value. Nevertheless, the intensity far from the front is shifted above the experimental value for the ZND simulation at D/D_{CJ}=1.2. The width of the Rayleigh intensity peak is much lower whatever the velocity of the ZND detonation is. The density jump across the one-dimensional shock is not very sensitive to velocity changes within the range we considered which is consistent with Anderson and Dabora observations. In order to match their lowest experimental density jump values, they had to consider a one-dimensional detonation propagating at D/D_{CJ}=0.5. This value seems quite low as compared to previous experimental [1] and numerical results [14, 15] which report lowest detonation speed of D/D_{CJ}=0.7 within a cell cycle. In order to match the highest density jump values they measured, Anderson and Dabora considered the density ratio resulting from the interaction of two opposing weak transverse waves. This indicates that the tridimensional structure of detonation waves has to be accounted for to perform meaningful comparisons with Anderson and Dabora's measurements. For instance, the Rayleigh intensity profiles extracted from 2-D simulations obtained previously by Davidenko et al. [8] better match the experimental results as seen in Figure 3 d). Note that the conditions differ between the experiment, P_1=37.4 kPa, T_1=295 K, $2H_2$-O_2-4Ar, and the simulation, P_1=20 kPa, T_1=295 K, $2H_2$-O_2-12Ar. Concerning the peak intensity, the comparison is satisfactory for the leading shock outline whereas the peak intensity at the triple point is under-estimated by 20% by the simulation. This can be explained by the fact that the experimental intensity was taken just after the merging of two triple points, whereas the calculated one was taken just before merging of the two triple points. It can also be noted that the width of the Rayleigh peaks are well reproduced by the simulation.

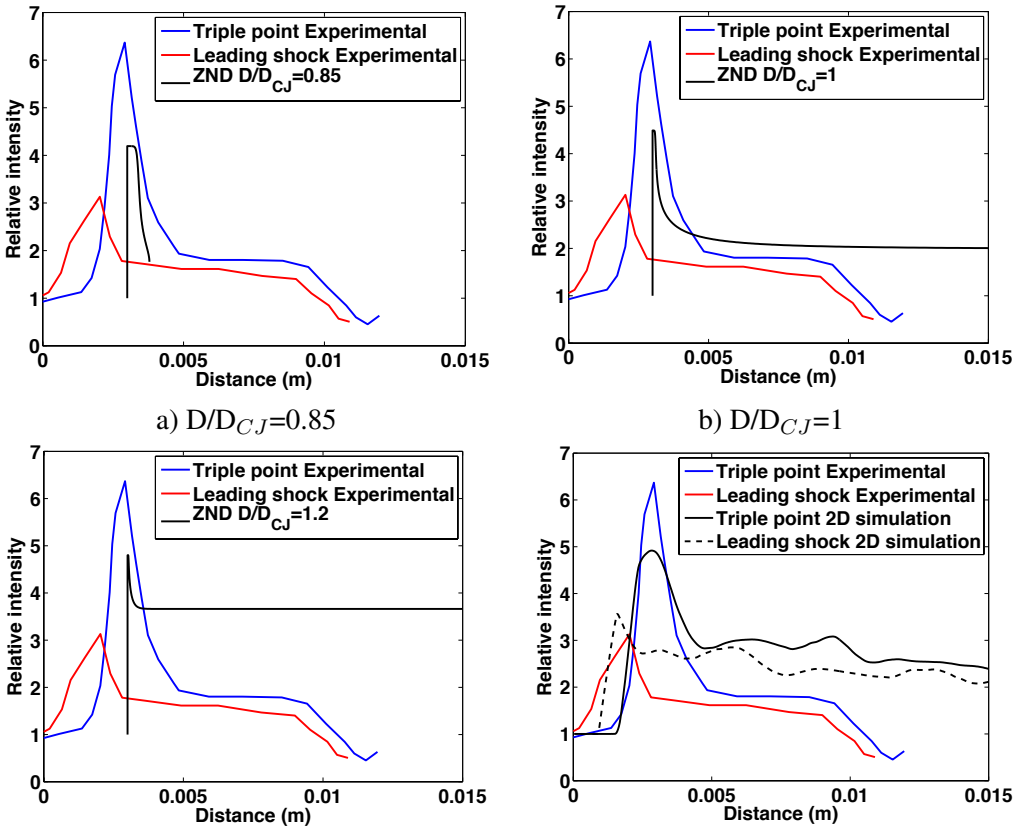

a) D/D_{CJ}=0.85 b) D/D_{CJ}=1

c) D/D_{CJ}=1.2 d) Intensity profiles from 2-D simulation

Figure 3: Comparison between the experimental [4] and calculated Rayleigh intensity from ZND, a) to c), and 2-D, d), simulations.

4 Conclusion

In the present study, the fundamentals of Rayleigh scattering phenomenon has been studied for application to the imaging of detonation waves.
In a first step, quantum chemistry has been employed to determine the Rayleigh cross-section of a large number of gaseous molecules. The database has been validated with respect to a variety of experimental data available in the literature. For most species, a relative errors smaller than 10% was found. A wavelength-dependent law for the variation of the Rayleigh scattering cross-section with temperature has been established based on previous experimental observations.
In a second step, Rayleigh intensity profiles and maps were calculated using 1-D steady and 2-D unsteady numerical results and compared to the experimental results from Anderson and Dabora. Overall agreement was found for the Rayleigh peak height and width in the case of the 2-D simulation. A number of real diagnostics effects have to be accounted for in order to reproduce closely the experimental images. The present approach, which combines realistic chemistry, fluid dynamics, spectroscopy, and real diagnostics effects, was demonstrated to be suitable to estimate the performance of a more modern imaging set-up. Rayleigh scattering appears to be an appropriate technique to study the structure of detonation waves both at and behind the front.

Acknowledgements
The authors are grateful to Dr T.J. Anderson who allowed us to reproduce his work in Figure 2.

References

[1] Austin J. (2003). Ph.D. thesis, California Institute of Technology.

[2] Pintgen F. (2000). Master's thesis, Technische Universität München and California Institute of Technology.

[3] Mével R. et al. (2014). International Journal of Hydrogen Energy 39: 6044.

[4] Anderson T.J. and Dabora E.K. (1992). Proceedings of the Combustion Institute 24: 1853.

[5] Zhao F.-Q. and Hiroyasu H. (1993). Progress in Energy and Combustion Science 19: 447.

[6] Pitts W. and Kashiwagi T. (1984). Journal of Fluid Mechanics 141: 391.

[7] Ponty L. (2011). Ph.D. thesis, Université d'Orléans.

[8] Davidenko D., Mével R. and Duprè G. (2011). Shock Waves 21: 85.

[9] Gardiner W.C., Hidaka Y. and Tanzawa T. (1981). Combustion and Flame 40: 213.

[10] Fielding J. et al. (2002). Proceedings of the Combustion Institute 29: 2703.

[11] Sutton J.A. and Driscoll J.F. (2004). Optics Letters 29: 2620.

[12] Graham S.C., Grant A.J. and Jones J.M. (1974). AIAA Journal 12: 1140.

[13] Holm U. and Kerl K. (1986). Molecular Physics 58: 541.

[14] Eckett C.A. (2001). Ph.D. thesis, California Institute of Technology.

[15] Gamezo V.N., Desbordes D. and Oran E.S. (1999). Combustion and Flame 116: 154.